

Northumbria Research Link

Citation: Hobson, Theodore D. C., Phillips, Laurie J., Hutter, Oliver, Durose, K. and Major, Jonathan D. (2020) Defect properties of Sb₂Se₃ thin film solar cells and bulk crystals. Applied Physics Letters, 116 (26). p. 261101. ISSN 0003-6951

Published by: American Institute of Physics

URL: <https://doi.org/10.1063/5.0012697> <<https://doi.org/10.1063/5.0012697>>

This version was downloaded from Northumbria Research Link:
<http://nrl.northumbria.ac.uk/id/eprint/43815/>

Northumbria University has developed Northumbria Research Link (NRL) to enable users to access the University's research output. Copyright © and moral rights for items on NRL are retained by the individual author(s) and/or other copyright owners. Single copies of full items can be reproduced, displayed or performed, and given to third parties in any format or medium for personal research or study, educational, or not-for-profit purposes without prior permission or charge, provided the authors, title and full bibliographic details are given, as well as a hyperlink and/or URL to the original metadata page. The content must not be changed in any way. Full items must not be sold commercially in any format or medium without formal permission of the copyright holder. The full policy is available online: <http://nrl.northumbria.ac.uk/policies.html>

This document may differ from the final, published version of the research and has been made available online in accordance with publisher policies. To read and/or cite from the published version of the research, please visit the publisher's website (a subscription may be required.)

Defect properties of Sb_2Se_3 thin film solar cells and bulk crystals

Cite as: Appl. Phys. Lett. **116**, 261101 (2020); <https://doi.org/10.1063/5.0012697>

Submitted: 04 May 2020 . Accepted: 22 June 2020 . Published Online: 01 July 2020

Theodore D. C. Hobson , Laurie J. Phillips , Oliver S. Hutter , K. Durose , and Jonathan D. Major 



View Online



Export Citation



CrossMark

ARTICLES YOU MAY BE INTERESTED IN

[In situ investigation of interfacial properties of \$\text{Sb}_2\text{Se}_3\$ heterojunctions](#)

Applied Physics Letters **116**, 241602 (2020); <https://doi.org/10.1063/5.0008879>

[Transition metals as optically active dopants in glass-ceramics](#)

Applied Physics Letters **116**, 260503 (2020); <https://doi.org/10.1063/5.0014618>

[Photonics based perfect secrecy cryptography: Toward fully classical implementations](#)

Applied Physics Letters **116**, 260502 (2020); <https://doi.org/10.1063/5.0010744>

 Measure Ready
FastHall™ Station

The highest performance tabletop system
for van der Pauw and Hall bar samples



Learn more

 Lake Shore
CRYOTRONICS

AIP
Publishing

Defect properties of Sb_2Se_3 thin film solar cells and bulk crystals

Cite as: Appl. Phys. Lett. **116**, 261101 (2020); doi: [10.1063/5.0012697](https://doi.org/10.1063/5.0012697)

Submitted: 4 May 2020 · Accepted: 22 June 2020 ·

Published Online: 1 July 2020



View Online



Export Citation



CrossMark

Theodore D. C. Hobson,¹  Laurie J. Phillips,¹  Oliver S. Hutter,²  K. Durose,¹  and Jonathan D. Major^{1,a)} 

AFFILIATIONS

¹Stephenson Institute for Renewable Energy, Department of Physics, University of Liverpool, Liverpool L69 7ZF, United Kingdom

²Department of Mathematics, Physics and Electrical Engineering, Northumbria University, Newcastle upon Tyne NE1 8QH, United Kingdom

^{a)} Author to whom correspondence should be addressed: jon.major@liverpool.ac.uk

ABSTRACT

As an absorber in photovoltaic devices, Sb_2Se_3 has rapidly achieved impressive power conversion efficiencies despite the lack of fundamental knowledge about its electronic defects. Here, we present a deep level transient spectroscopy (DLTS) study of deep level defects in both bulk crystal and thin film device material. DLTS study of Bridgman-grown *n*-type bulk crystals revealed traps at 358, 447, 505, and 685 meV below the conduction band edge. Of these, the energetically close pair at 447 and 505 meV could only be resolved using the isothermal transient spectroscopy (rate window variation) method. A completed Sb_2Se_3 thin film solar cell displayed similar trap spectra with traps identified at 378, 460, and 690 meV. The comparable nature of defects in thin film and bulk crystal material implies that there is minimal impact of polycrystallinity in Sb_2Se_3 supporting the concept of benign grain boundaries.

Published under license by AIP Publishing. <https://doi.org/10.1063/5.0012697>

Defects are one of the key controlling factors for performance in photovoltaic (PV) devices. They control the doping level of the material, carrier lifetime, and the rate of interfacial recombination. This is particularly problematic for polycrystalline thin film solar cells, where the material quality and structure are far less controlled than for wafer technologies, such as Si or GaAs. Owing to the rapid deposition methods used¹ and the often-low purity starting materials,² these devices have to contend not only with the presence of native defects³ but also with uncontrolled impurities arising from various sources, such as out diffusion of impurities from glass substrates.⁴ There is also the additional complication of grain boundaries since thin film photovoltaic (PV) absorbers are invariably polycrystalline, which may further complicate the defect picture.⁵ The ability to understand problematic native defects, in particular, allows the next step of cell development to be identified. This can be exemplified by the passivation of Te_i defects in CdTe via a chloride treatment^{6,7} and the use of NaF and KF in $\text{CuIn}_x\text{Ga}_{(1-x)}\text{Se}_2$ (CIGS) to modify interface states⁸ and of Zn:Cu cation disorder issue in $\text{Cu}_2\text{ZnSnS}_4$ (CZTS),⁹ which motivated the development of Ag cation substitution¹⁰ to compensate for the antisite defects.¹¹ Understanding the defect properties is a first but vital step in improving a PV material.

Antimony selenide, Sb_2Se_3 , solar cells are one of the newer thin film technologies but have already achieved a 9.2% efficiency.¹² Sb_2Se_3

has a 1.18 eV direct bandgap with strong optical absorption¹³ and contains no highly toxic or low abundance elements such as In, Te, Cd, or Pb. It has been suggested that the material nano-ribbon structure¹⁴ should minimize the influence of grain boundaries¹² and that the material may even be defect tolerant.¹⁵ Recent density functional theory work has highlighted the potential complex nature of antimony selenide defects,¹⁶ but thus far, there has been minimal experimental work on the defect composition of Sb_2Se_3 .

In this paper, we report on the analysis of electrically active defects via deep level transient spectroscopy (DLTS) in both complete Sb_2Se_3 solar cells and bulk crystal Sb_2Se_3 . This analysis shows the presence of significant deep levels with spectra for bulk crystals and solar cells nearly identical, indicating that the presence of grain boundaries has only a minimal influence on the defect composition of Sb_2Se_3 solar cells.

The solar cell structure used was glass/ SnO_2 :F/ TiO_2 / Sb_2Se_3 /Au. TiO_2 layers were deposited via spin coating onto an NSG TEC 15 FTO coated glass.¹⁷ Sb_2Se_3 layers were deposited via close spaced sublimation (CSS) using a two-stage process comprising a low temperature step to produce a compact “seed” layer followed by a second higher temperature stage to achieve large grains with an optimized ribbon orientation.¹⁸ Gold back contacts were added via thermal evaporation.

Sb_2Se_3 bulk crystal samples were grown using a Bridgman melt-growth method. 4 mm diameter quartz tubes were filled with ~ 7 g of

Sb₂Se₃ powder (5N purity from Alfa Aesar) before being argon flushed and then evacuated to 10⁻⁵ mbar and sealed. Sealed ampoules were then lowered into a vertical single-zone furnace with the ampoule tip being held at the peak temperature point of 615 °C, set to be just above the 611 °C melting point of Sb₂Se₃.¹⁹ It has a lowering rate of 1.15 mm/h through the furnace for seven days with a temperature gradient of 6 °C/cm.²⁰ Crystals were cleaved in one direction to reveal flat, parallel reflective single-crystal facets. XRD measurements on identical cleaved facets are reported in the work of Fleck *et al.*²¹ and demonstrated diffraction peaks corresponding to the {010} plane family only, confirming that the cleaved pieces were single crystals, with the (010) plane exposed by the cleavage. The sample examined in this work was of identical form with the electrodes placed on the (010) plane.

A ~0.5 mm thick slice was taken from the bulk crystal, and gold contacts were applied to form a Schottky junction with the n-type Sb₂Se₃ and allow the DLTS measurement.

Device performance of the Sb₂Se₃ was assessed via current–voltage (J–V) analysis prior to DLTS measurements under a simulated AM1.5 spectrum using a TS space system simulator.

DLTS measurements were performed using a Phystech FT1230 HERA DLTS system linked to a Linkam HFSX350 liquid nitrogen fed cryostat. Capacitance transients due to depopulation of trap levels were recorded, and time constants were determined for a range of correlator functions.²² Data were recorded from 80 K upwards; however, the measurement of <150 K produced no good quality capacitance transients. Determination of the emission time constants as a function of temperature allowed the production of Arrhenius plots, from which the trap energy, E_T , and capture cross section can be determined via assessment of the electron trap emission time constants, τ_e , as per the following equation:

$$\tau_e = \left[(\sigma_n \nu_{th} N_c) e^{-\frac{E_T}{kT}} \right]^{-1}, \quad (1)$$

where σ_n is the capture cross section for holes, E_T is the energy of the trap level (with respect to the valence band for holes), T is the temperature, N_c is the effective density of states in the conduction band, and ν_{th} is the electron thermal velocity.

The concentration of trap levels, N_T , was determined from the magnitude of the trap-related capacitance change, ΔC , relative to the capacitance at reverse bias, C_R , and the shallow doping density of the material, N_s , via the following equation:

$$N_T = 2N_s \frac{\Delta C}{C_R}. \quad (2)$$

For a detailed review of the underpinning theory of DLTS analysis, the reviewer is referred to the comprehensive review article by Peaker *et al.*²³

Prior to DLTS analysis, CV measurements were performed on both the solar cell and bulk crystal samples to establish the shallow doping density, N_s . The solar cell sample was found to have a much higher doping density in the 10¹⁶–10¹⁷ cm⁻³ range compared to the bulk crystal sample 10¹¹–10¹² cm⁻³. Both the thin film and bulk crystal material had been determined as n-type,²⁴ due to the presence of shallow Cl-dopant levels; hence, all trap energies were measured with respect to the conduction band. Additionally, for the solar cell sample, JV analysis was performed on the measured contact to check the level

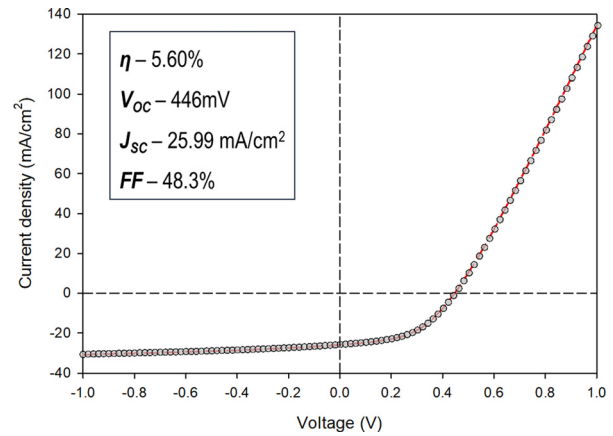


FIG. 1. Current–voltage analysis of a thin film solar cell used for DLTS analysis with extracted device performance parameters (inset).

of device performance (Fig. 1). The cell was found to operate at a 5.6% efficiency with a good open circuit voltage of 446 mV.

Figure 2 shows DLTS measurements recorded for both the bulk crystal [Fig. 2(a)] and solar cell sample [Fig. 2(b)], with both samples displaying three distinct peaks, labeled E1–E3. Arrhenius plots determined from the variation of these peaks with the correlator function and period width are shown in Figs. 2(c) and 2(d), with the extracted parameter values given in Table I.

The evaluation of levels E1 and E3 is straightforward and confirms them to be the same levels in both the bulk crystal and thin film variants. Level E1 is located at 358–378 meV below the conduction band, with a capture cross section of $\sim 10^{-14}$ cm². The trap density for the E1 level was $\sim 10^{14}$ cm⁻³ in the solar cell device, but for the bulk crystal sample, it could not be accurately calculated owing to the low magnitude of the reverse capacitance signal at this temperature range. The E3 level shows similar good agreement between the sample types at 685–690 meV and is a more problematic mid-gap level. It was consistently found as the dominant defect level in all solar cells and bulk crystal samples measured.

The energetic position of the E2 level initially appeared more variable, being determined as significantly deeper, >700 meV, in the bulk crystal than for the solar cell sample at 460 meV (Table I). Indeed, across the whole range of measurement parameters compared for the samples (i.e., various pulse/period widths), at no point did the E2 trap energies determined via Arrhenius assessment coincide between the sample types. Given the shape of the DLTS spectra in both cases, and the consistent positioning with respect to E1 and E3 levels, it was considered unlikely that the E2 level had different origins in the two sample types. A much higher capture cross section was also observed for the bulk crystal E2 level than for all other determined levels, at $\sim 10^{-11}$ cm². This was indicative of the closely spaced levels with overlapping time constants being present around the E2 level position. This can have the influence of appearing to create an artificially¹⁸ extended time constant, giving rise to an erroneously elevated trap energy if assessed as a single level. The separation of closely spaced energy levels can be problematic, but there are a number of approaches that can be taken to do so (e.g., Laplace DLTS²⁵). Here, we have employed a variant of DLTS, isothermal transient spectroscopy (ITS),²⁶ to separate the levels.

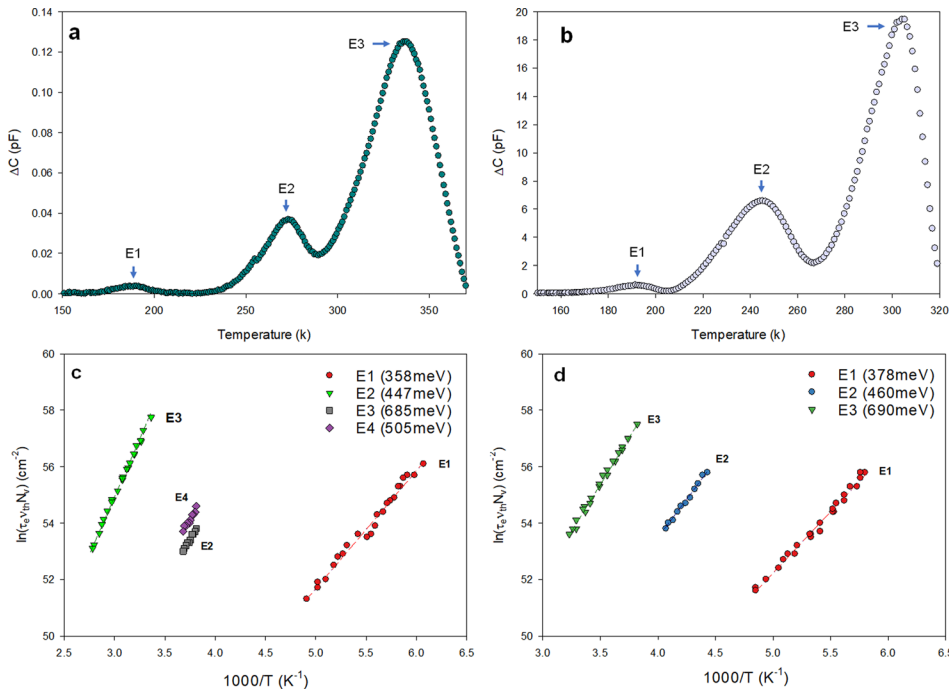


FIG. 2. DLTS analysis of (a) Sb_2Se_3 bulk crystal and (b) thin film solar cell with Arrhenius plots extracted for (c) Sb_2Se_3 bulk crystal and (d) thin film solar cell.

ITS uses the same theoretical basis as the standard DLTS analysis [i.e., Eq. (1)] but differs, in that the sample is held at a constant temperature while the period width over which the capacitance transient is assessed is varied, in this instance from 0.6 ms to 500 ms. For a given temperature, the capacitance change, ΔC , will reach a maximum when the emission time constant, τ_e , of a defect level matches the period width of the measurement.²² This produces maxima at a specific period width for a given trap for each temperature measured, similar to a standard DLTS measurement, as shown in Fig. 3. By measuring successive ITS spectra at different temperatures, a comparative Arrhenius style assessment can be performed but with higher energy resolution. ITS scans were performed for temperatures at which the E2 peak was observable in the standard DLTS measurement. Whereas for the thin film sample [Fig. 3(b)], there is still an apparent single dominant level, for the single crystal sample [Fig. 3(a)], two separate peaks, labeled E2

and E4, are resolved. These peaks were used to update the Arrhenius data for the E2 peak in the single crystal sample [Fig. 2(c) and Table I]. The E2 peak energy for the single crystal sample was determined to be at 447 ± 22 meV from the ITS measurement, with a capture cross section in the 10^{-14} cm² range, in good agreement with the thin film sample. Prior assessment had been compromised by the presence of the E4 level at ~ 505 meV. Again, we were unable to accurately assess the N_T density values for these trap states due to the low pulse capacitance change in relation to the reverse capacitance. Additional ITS analysis using a shorter pulse width, 100 μs , and an alternative correlator function with higher energy resolution also resolved the E4 level in the thin film sample [see Fig. 3(c)]. However, the low signal to noise ratio did not allow an energy value to be extracted via Arrhenius assessment and thus confirm definitively.

From this analysis, it is apparent that both crystals and thin films of Sb_2Se_3 share a common electrically active defect composition. Three significant trap states, E1–E3, are present in single crystals and persist into the solar cell. A fourth level, E4, is resolved for the single crystal, with the crystal also seemingly being present but difficult to characterize in the thin film. All defect levels observed are relatively deep, with E2–E4 being near the mid gap, which we would expect to strongly limit the performance. Prior DLTS work on Sb_2Se_3 solar cells by Wen *et al.*²⁷ identified only a single electron trap state at 0.60–0.61 eV below the conduction band, but also a number of hole traps in close proximity on the temperature scan. Direct comparison of results presented here is difficult as Wen *et al.* identify their material as being *p*-type rather than *n*-type. Additionally in a standard DLTS analysis probes only majority carrier states, with optical DLTS analysis usually required to assess minority states. While minority carrier peaks can be achieved by the use of injection DLTS methods, as employed by Wen *et al.*, extreme care must be taken to ensure that they do not result

TABLE I. Extracted DLTS trap parameters for bulk crystal and solar cell samples. Trap energies are with respect to the conduction band.

	E_T (meV)	σ (cm ²)	N_T (cm ⁻³)
E1—Crystal	358 ± 13	$(0.99\text{--}3.79) \times 10^{-14}$...
E2—Crystal	447 ± 22	$(0.18\text{--}1.58) \times 10^{-14}$...
E3—Crystal	685 ± 8	$(1.00\text{--}2.95) \times 10^{-13}$	$(1.99\text{--}2.79) \times 10^{11}$
E4—Crystal	505 ± 12	$(1.04\text{--}2.36) \times 10^{-14}$...
E1—Cell	378 ± 8	$(3.83\text{--}7.05) \times 10^{-14}$	$(0.98\text{--}1.10) \times 10^{14}$
E2—Cell	460 ± 15	$(1.54\text{--}1.97) \times 10^{-14}$	$(4.15\text{--}8.71) \times 10^{14}$
E3—Cell	690 ± 5	$(2.21\text{--}9.66) \times 10^{-14}$	$(1.18\text{--}2.61) \times 10^{15}$

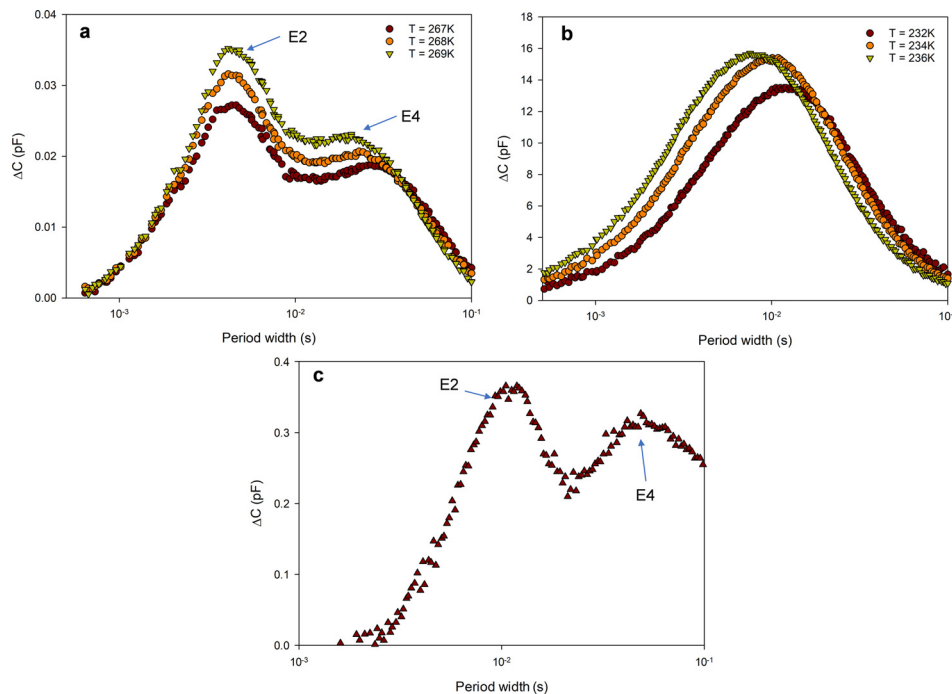


FIG. 3. Isothermal transient spectroscopy (ITS) analysis of (a) Sb_2Se_3 bulk crystal and (b) Sb_2Se_3 thin film solar cell with (c) ITS analysis of the solar cell using a smaller pulse width and a higher resolution ITS correlator function at 234 K.

from artifact related to either a back contact barrier²⁸ or from a change in the reverse capacitance, which cannot be compensated for when using a short measurement period width.²⁹ Under the measurement conditions employed in this work, minority carrier peaks could not be observed.

The similarity of defects in single crystal and thin film solar cell is somewhat unexpected. The expectation would be that the switch to a less refined polycrystalline solar cell would induce significant additional defect states. Conversely though, for DLTS analysis, we would expect that defects in single crystal material would be more clearly resolved when there is no interference from grain boundary electric fields. The fact that, from the analysis conducted here, polycrystalline Sb_2Se_3 thin films behave like single crystals may be the reason for their good performance. In effect, Sb_2Se_3 solar cells appear to act as pseudo single crystal devices. This is consistent with the concept of grain boundaries in the material being non-limiting due to good orientation of the nano-ribbon structure¹² and the self-healing effect observed at grain boundaries.³⁰ However, despite the lack of apparent influence from the grain boundaries, the material still contains a significant content of deep levels. The fact that the devices used here functioned in excess of 6% efficiency would imply some degree of overall defect tolerance in the material, something that has been previously suggested for ns (Ref. 2) containing materials such as this.¹⁵ Clearly though, these defect levels are undesirable, so routes to engineer out or pacify them should be sought, meaning identification of these defects is of paramount importance. Comparison with formation energy calculations provides some guidance, but definitive identification of the exact defect center types is difficult given the complexity of the predicted formation energies.^{16,24} There are numerous potential midgap states resulting from both native defects (e.g., Se_{Sb} and V_{Se}) and dopant interstitials (i.e., Cl_i), meaning any conclusive identification by simple comparison with theory is not possible with any degree of confidence. A large

amount of further work will be required to identify and thus control the defect composition of Sb_2Se_3 —this will, however, be the key route to improved solar cell performances through increased carrier recombination.

To summarize, we have performed a comparative DLTS assessment of electrically active defect levels in Sb_2Se_3 single crystals and thin film solar cells. Both material types show common deep level signatures in the 358–690 meV range below the conduction band edge. The lack of variation between the thin film and single crystal equivalents implies minimal influence on defect composition from the presence of grain boundaries in the thin film material. The chemical identity of these defects is not able to be identified at this time; however, they will likely remain limiting to solar cell performance. As such, identification and elimination of the determined defects represent the key ongoing work for the development of the technology.

We acknowledge the engineering and physical sciences research council for funding via Grant Nos. EP/N01457/1, EP/L01551X/1, and EP/M024768/1.

DATA AVAILABILITY

Data files related to the project are available from <http://datacat.liverpool.ac.uk/id/eprint/1080> or from the corresponding author.

REFERENCES

- ¹J. D. Major, Y. Y. Proskuryakov, K. Durose, G. Zoppi, and I. Forbes, *Sol. Energy Mater. Sol. Cells* **94**, 1107 (2010).
- ²M. Emziane, K. Durose, N. Romeo, A. Bosio, and D. P. Halliday, *Semicond. Sci. Technol.* **20**, 434 (2005).
- ³D. J. Keeble, J. D. Major, L. Ravelli, W. Egger, and K. Durose, *Phys. Rev. B* **84**, 174122 (2011).
- ⁴M. Emziane, K. Durose, D. P. Halliday, N. Romeo, and A. Bosio, *Thin Solid Films* **511-512**, 66 (2006).

- ⁵J. D. Major, *Semicond. Sci. Technol.* **31**, 093001 (2016).
- ⁶J. D. Major, M. Al Turkestani, L. Bowen, M. Brossard, C. Li, P. Lagoudakis, S. J. Pennycook, L. J. Phillips, R. E. Treharne, and K. Durose, *Nat. Commun.* **7**, 1–10 (2016).
- ⁷C. Li, Y. Wu, J. Poplawsky, T. J. Pennycook, N. Paudel, W. Yin, S. J. Haigh, M. P. Oxley, A. R. Lupini, M. Al-Jassim, S. J. Pennycook, and Y. Yan, *Phys. Rev. Lett.* **112**, 156103 (2014).
- ⁸A. Chirilă, P. Reinhard, F. Pianezzi, P. Bloesch, A. R. Uhl, C. Fella, L. Kranz, D. Keller, C. Gretener, H. Hagendorfer, D. Jaeger, R. Erni, S. Nishiwaki, S. Buecheler, and A. N. Tiwari, *Nat. Mater.* **12**, 1107 (2013).
- ⁹B. G. Mendis, M. D. Shannon, M. C. Goodman, J. D. Major, R. Claridge, D. P. Halliday, and K. Durose, *Prog. Photovoltaics* **22**, 24 (2014).
- ¹⁰J. Li, D. Wang, X. Li, Y. Zeng, and Y. Zhang, *Adv. Sci.* **5**, 1700744 (2018).
- ¹¹S. Chen, A. Walsh, X.-G. Gong, and S.-H. Wei, *Adv. Mater.* **25**, 1522 (2013).
- ¹²Y. Zhou, L. Wang, S. Chen, S. Qin, X. Liu, J. Chen, D.-J. Xue, M. Luo, Y. Cao, Y. Cheng, E. H. Sargent, and J. Tang, *Nat. Photonics* **9**, 409 (2015).
- ¹³M. Birkett, W. M. Linhart, J. Stoner, L. J. Phillips, K. Durose, J. Alaria, J. D. Major, R. Kudrawiec, and T. D. Veal, *APL Mater.* **6**, 084901 (2018).
- ¹⁴L. J. Phillips, C. N. Savory, O. S. Hutter, P. J. Yates, H. Shiel, S. Mariotti, L. Bowen, M. Birkett, K. Durose, D. O. Scanlon, and J. D. Major, *IEEE J. Photovoltaics* **9**, 544 (2019).
- ¹⁵A. M. Ganose, C. N. Savory, and D. O. Scanlon, *Chem. Commun.* **53**, 20 (2017).
- ¹⁶C. N. Savory and D. O. Scanlon, *J. Mater. Chem. A* **7**, 10739 (2019).
- ¹⁷S. Mariotti, O. S. Hutter, L. J. Phillips, P. J. Yates, B. Kundu, and K. Durose, *ACS Appl. Mater. Interfaces* **10**, 3750 (2018).
- ¹⁸O. S. Hutter, L. J. Phillips, K. Durose, and J. D. Major, *Sol. Energy Mater. Sol. Cells* **188**, 177 (2018).
- ¹⁹G. Ghosh, *J. Phase Equilib.* **14**, 753 (1993).
- ²⁰T. D. C. Hobson, O. S. Hutter, M. Birkett, T. D. Veal, and K. Durose, in *IEEE Photovoltaics Specialist Conference, Hawaii* (2018), pp. 3–7.
- ²¹N. Fleck, T. D. C. Hobson, C. N. Savory, J. Buckeridge, T. D. Veal, M. R. Correia, D. O. Scanlon, K. Durose, and F. Jäckel, *J. Mater. Chem. A* **8**, 8337 (2020).
- ²²S. Weiss and R. Kassing, *Solid-State Electron.* **31**, 1733 (1988).
- ²³A. R. Peaker, V. P. Markevich, and J. Coutinho, *J. Appl. Phys.* **123**, 161559 (2018).
- ²⁴T. D. C. Hobson, L. J. Phillips, O. S. Hutter, H. Shiel, J. E. N. Swallow, C. N. Savory, P. K. Nayak, S. Mariotti, B. Das, L. Bowen, L. A. H. Jones, T. J. Featherstone, M. J. Smiles, M. A. Farnworth, G. Zoppi, P. K. Thakur, T. L. Lee, H. J. Snaith, C. Leighton, D. O. Scanlon, V. R. Dhanak, K. Durose, T. D. Veal, and J. D. Major, *Chem. Mater.* **32**, 2621 (2020).
- ²⁵V. Kolkovskiy, L. Dobaczewski, K. B. Nielsen, V. Kolkovskiy, A. N. Larsen, and J. Weber, *Physica B* **404**, 5080 (2009).
- ²⁶H. Okushi and Y. Tokumaru, *Jpn. J. Appl. Phys., Part 2* **19**, L335 (1980).
- ²⁷X. Wen, C. Chen, S. Lu, K. Li, R. Kondrotas, Y. Zhao, W. Chen, L. Gao, C. Wang, J. Zhang, G. Niu, and J. Tang, *Nat. Commun.* **9**, 2179 (2018).
- ²⁸J. Van Gheluwe and P. Clauws, *Thin Solid Films* **515**, 6256 (2007).
- ²⁹D. S. Day, M. Y. Tsai, B. G. Streetman, and D. V. Lang, *J. Appl. Phys.* **50**, 5093 (1979).
- ³⁰R. Williams, Q. M. Ramasse, K. P. McKenna, L. J. Phillips, P. Yates, O. Hutter, K. Durose, J. D. Major, and B. G. Mendis, *ACS Appl. Mater. Interfaces* **12**, 21730 (2020).